OPEN ACCESS

University of BRISTOL

Gill, S. J., Lowenberg, M. H., Neild, S. A., Crespo, L., Krauskopf, B., & Puyou, G. (2015). Nonlinear Dynamics of Aircraft Controller Characteristics Outside the Standard Flight Envelope. *Journal of Guidance, Control, and Dynamics*, *38*(12), 2301-2308. https://doi.org/10.2514/1.G000966

Peer reviewed version

Link to published version (if available):
10.2514/1.G000966

Link to publication record in Explore Bristol Research
PDF-document

University of Bristol - Explore Bristol Research
General rights

This document is made available in accordance with publisher policies. Please cite only the published version using the reference above. Full terms of use are available:
http://www.bristol.ac.uk/red/research-policy/pure/user-guides/ebr-terms/

Nonlinear Dynamics of Aircraft Controller Characteristics Outside the Standard Flight Envelope

Stephen J. Gill[1], Mark H. Lowenberg[2] and Simon A. Neild[3]
University of Bristol, Bristol, BS8 1TR, UK

Luis G. Crespo[4]
National Institute of Aerospace, 100 Exploration Way, Hampton VA 23666 USA

Bernd Krauskopf[5]
University of Auckland, Private Bag 92019, Auckland, 1142, New Zealand

Guilhem Puyou[6]
Airbus France, 31060 Toulouse Cedex 03, France.

In this paper the influence of the flight control system over the off-nominal flying dynamics of a remotely operated air vehicle is evaluated. Of particular interest is the departure/upset behaviour of the closed-loop system near stall. The study vehicle is the NASA Generic Transport Model and both fixed-gain and gain-scheduled versions of a linear quadratic regulator controller with proportional and integral components are evaluated. Bifurcation analysis is used to characterize spiral and spin behaviour of the aircraft in closed-loop form and yields an understanding of the underlying vehicle dynamics outside the standard flight envelope. The use of a 'gain parameter' to scale the controller gains provides information on the sensitivity of stability to gain variation along with tracking how the controller modifies the open-loop steady states. Hence, this provides a means of assessing the effectiveness of the controller and evaluating the upset tendencies of the aircraft.

---

[1] PhD Student, Departments of Aerospace Engineering and AIAA Member.
[2] Professor of Flight Dynamics, Department of Aerospace Engineering, and AIAA Senior Member.
[3] Professor in Nonlinear Structural Dynamics, Department of Mechanical Engineering.
[4] Associate Research Fellow, AIAA Senior Member.
[5] Professor of Applied Mathematics, Department of Mathematics, Faculty of Science.
[6] Airbus Research and Technology, Toulouse.

I. Introduction

Despite the relatively complex control laws in place on modern fly-by-wire airliners [1] that aim to maintain a safe operating envelope, the problem of airliners encountering upset phenomena leading to loss-of-control (LOC) still persists [2]. This is characterised by a flight trajectory involving large deviations in attitude and angular rates. During such excursions, the aircraft dynamics are dominated by aerodynamic forces and torques that are strongly nonlinear and might be coupled with the moments of inertia and pilot commands. It is often of interest to determine if the flight controller plays a beneficial role on the recovery from vehicle upsets. Typically controllers are often based on linear time-invariant (LTI) models, however, these are of limited value when analysing nonlinear systems. Unfortunately, most of the mathematical tools for control analysis are based on such models [3].

A variety of control design approaches have been developed to overcome the limitations of linear controllers. A popular approach is gain-scheduling, where a set of linear controllers are designed at several operating points and then blended together with respect to an input or state variable [4]. They do, however, usually suffer the limitation of being designed only at trim points within the expected operating envelope and, hence, may not cope well with nonlinearity under off-nominal conditions. Also, care needs to be exercised when scheduling with respect to a state variable that changes rapidly. To overcome the limitations of linearity, much work has been done on nonlinear control law design, such as by dynamic inversion [5] and a host of adaptive techniques [6, 7]. These are also not necessarily problem-free, with issues such as robustness to model uncertainty and stability guarantees requiring special attention. Typically, nonlinear controllers are also evaluated only under nominal operating conditions (i.e. those within the expected operating range, and up to the stall), partly because this is how the design requirements are stipulated.

Whether implementing gain-scheduled control or another nonlinear approach, a suitably representative mathematical model is needed. Due to the increased nonlinearity and time-dependence inherent in flight dynamics behaviour under off-nominal conditions – particularly at high angles of attack and/or sideslip – such models are more difficult and expensive to create than conventional models and will inevitably incorporate far higher levels of uncertainty. Hence, they do not generally exist for civil aircraft. However, researchers at NASA Langley have created the Generic Transport Model (GTM): this represents a dynamically scaled version of a twin-engine jet vehicle with a geometry characteristic of low-wing airliners with under-wing-

mounted engines [8]. The purpose of the model, derived from a comprehensive wind tunnel test campaign as well as from remotely piloted tests of a powered flight vehicle, was indeed to generate a representative wide-envelope airliner flight dynamics model for the simulation and analysis of upset and LOC [9]. A similar model was created for the EU 'Simulation of UPset Recovery in Aviation' (SUPRA) research programme [10].

The use of continuation and bifurcation analysis methods for flight dynamics and control applications is well defined; see [11] and [12] for comprehensive surveys of bifurcation analysis applied to fixed-wing flight dynamics and control problems. However this analysis has largely focused on military aircraft. This approach has recently been implemented, for commercial airliners, on the NASA Generic Transport Model (GTM) [13] and the SUPRA model [10] in open-loop form, and has revealed spiral dives and steep spins.

This paper extends the bifurcation analysis performed in [13] to analyse the dynamics of the GTM coupled to closed loop controllers. Two linear quadratic regulator with proportional and integral components (LQR-PI) controllers, described in [14], are considered, the first with fixed-gains and the second with gain-scheduling implemented. We investigate how these controllers affect the flight dynamics of the GTM. Then, we look at the sensitivity of the flight dynamics to the controller gains to determine the robustness in behaviour off-nominal to the controller design and to gain insight into the components of the controller that are critical in preventing upset.

The paper is organized as follows. In Section II the aircraft model and controller architecture are described and their performance briefly compared using time responses. In Section III the bifurcation analysis of the open-loop GTM is summarised, with an emphasis on upset behaviour; an assessment is then made of the changes in the system attractors as the control loop is closed, focusing on the spiral and spin solutions and their respective stability characteristics. Finally, in Section IV, conclusions are drawn concerning the changes in off-nominal attractors arising from using a control law, hence, the benefits offered by bifurcation methods in evaluating closed-loop flight dynamics.

II. Plant and Controller Architecture

A. The Generic Transport Model

The GTM is a model of a commercial transport aircraft for which both a dynamically scaled flight test vehicle and a high-fidelity simulation model were developed. References [8, 15, 16] provide details of the vehicle's configuration and characteristics and the flight experiments. The aircraft is piloted from a ground station via radio frequency links by using onboard cameras and synthetic vision technology.

The high-fidelity simulation model, known as the DesignSim, uses nonlinear aerodynamic models extracted from wind tunnel data and system identification for conditions that include high angles of attack, and considers actuator dynamics with rate and range limits, engine dynamics, sensor dynamics along with analog-digital-analog latencies and quantization, sensor noise and biases, telemetry uplink and downlink time delays, turbulence, atmospheric conditions, etc.

B. Control Design

Analysis of both a fixed-gain and a gain-scheduled controller are considered in this paper. These controllers are surmised below; for further details see Ref. [14] and, for the fixed-gain controller, Ref. [7] where it is refereed to as the 'baseline controller'. The system dynamics can be represented as

$$\dot{X} = F(X, U), \tag{1}$$

where F is a nonlinear function of the state vector X and the control input U. For control design purposes, this nonlinear plant is linearized about a trim point (X^*, U^*) satisfying $F(X^*, U^*) = 0$ for the force and moment equations. Deviations from the trim values X^* and U^* are written as lower-case letters hereafter, e.g., $X = X^* + x_p$ and $U = U^* + u$. Linearization of Eq. (1) about the trim point leads to the system

$$\dot{x}_p = A_p x_p + B_p u + \nu(x_p, u), \text{ where: } A_p = \left.\frac{\partial F}{\partial X}\right|_{X^*, U^*}, \quad B_p = \left.\frac{\partial F}{\partial U}\right|_{X^*, U^*}, \tag{2}$$

and ν contains higher-order terms. In a sufficiently small neighbourhood of the trim point, the effect of the higher-order terms is negligible. The LTI representation of the plant, which results from dropping the higher-order terms from Eq. (2), is given by

$$\dot{x}_p = A_p x_p + B_p(R_s(u) + d) + B_2 \hat{r}, \tag{3}$$

where A_p and B_p are the system and control input matrices, $d(t)$ is an exogenous disturbance; $\hat{r}(t)$ is the reference command generated by the pilot; $R_s(u)$ is a saturation function that enforces range saturation limits in the control inputs, and B_2 is the command input matrix.

The states, x_p, consists of $[\alpha, \beta, V, p, q, r, x, y, z, \phi, \theta, \psi]$ where α is the angle of attack, β is the sideslip angle, V is the velocity, $[p, q, r]$ are the roll, pitch and yaw angular velocities, $[x, y, z]$ are the translational states and $[\phi, \theta, \psi]$ are the roll, pitch and yaw euler angles. The control input u consists of the the elevator, aileron and rudder deflections $[\delta_e, \delta_a, \delta_r]$ and the throttle input to the engines, δ_{th}. The reference command $\hat{r}$ consists of angle of attack-, sideslip-, speed- and roll rate-commands, denoted as α_{cmd}, β_{cmd}, V_{cmd}, and p_{cmd}, respectively. The flight controller consists of independent controllers for the longitudinal and the lateral/directional dynamics. The controllers operating the control surfaces are based on LQR-PI terms having integral error states for the reference commands. The throttle input to the engines, which is in the form of a deviation from a trim value, was prescribed by a simple proportional-derivative auto-throttle controller. The regulation of airspeed and pitch control were done separately because of a large time scale separation between the corresponding actuators.

1. Longitudinal Controller

The linearized plant for pitch control takes the form $\dot{x}_{\text{lon}} = A_{\text{lon}} x_{\text{lon}} + B_{\text{lon}} u_{\text{lon}}$ where $A_{\text{lon}} \in \mathbb{R}^{3\times 3}$ is the system matrix, $B_{\text{lon}} \in \mathbb{R}^{3\times 1}$ is the input matrix, $x_{\text{lon}} = [\alpha\ q\ V]^\top$ is the state, and $u_{\text{lon}} = \delta_e$ is the input. To enable tracking commands in angle of attack, an integral error in angle of attack error e_α was added, giving the augmented plant

$$\begin{bmatrix} \dot{x}_{\text{lon}} \\ \dot{e}_\alpha \end{bmatrix} = \left[\begin{array}{c|c} A_{\text{lon}} & 0 \\ \hline 1\,0\,0 & 0 \end{array}\right] \left[\begin{array}{c} x_{\text{lon}} \\ \hline e_\alpha \end{array}\right] + \begin{bmatrix} B_{\text{lon}} \\ 0 \end{bmatrix} \delta_e + \begin{bmatrix} 0 \\ -1 \end{bmatrix} \alpha_{\text{cmd}}. \tag{4}$$

A constant gain LQR controller that minimizes

$$J = \int_0^\infty (x_{\text{lon}}^T Q x_{\text{lon}} + \delta_e^2 R) dt, \tag{5}$$

where $Q = Q^\top \geq 0$, $R > 0$ are weighting matrices, was designed. This led to $u_{lon} = \delta_e = K_{\text{lon}} x_{\text{lon}} + K_{e\alpha} e_\alpha$. This controller must attain ample stability margins so the low-pass- and anti-aliasing-filters from sensors and the delay caused by telemetry do not compromise stability.

The plant's input is given by $R_s(u) = u$ with lower and upper actuator saturation limits of u_{min} and u_{max} respectively. Based on the saturation limits, the integrator anti-windup strategy proposed in [7] is applied to the $\langle e_\alpha, \delta_e \rangle$ pair.

2. Lateral/Directional Controller

An LTI model of the corresponding plant is $\dot{x}_{\text{lat}} = A_{\text{lat}} x_{\text{lat}} + B_{\text{lat}} u_{\text{lat}}$, where $A_{\text{lat}} \in \mathbb{R}^{3\times 3}$ is the system matrix, $B_{\text{lat}} \in \mathbb{R}^{3\times 2}$ is the input matrix, $x_{\text{lat}} = [\beta\ p\ r]^\top$ is the state, and $u_{\text{lat}} = [\delta_a\ \delta_r]^\top$ is the input. To enable satisfactory command following, integral error states for sideslip,e_β, and roll rate, e_p, were added. The integral error in sideslip was chosen over that of the yaw rate to facilitate the generation of commands for coordinated turns with non-zero bank angles and cross-wind landing. The augmented plant is given by

$$\begin{bmatrix} \dot{x}_{\text{lat}} \\ \dot{e}_\beta \\ \dot{e}_p \end{bmatrix} = \left[\begin{array}{ccc|c} \multicolumn{3}{c|}{A_{\text{lat}}} & 0 \\ \hline 1 & 0 & 0 & 0 \\ 0 & 1 & 0 & 0 \end{array}\right] \left[\begin{array}{c} x_{\text{lat}} \\ \hline e_\beta \\ e_p \end{array}\right] + \begin{bmatrix} B_{\text{lat}} \\ 0 \\ 0 \end{bmatrix} u_{\text{lat}} + \begin{bmatrix} 0 \\ -I \end{bmatrix} \begin{bmatrix} \beta_{\text{cmd}} \\ p_{\text{cmd}} \end{bmatrix}, \tag{6}$$

A LQR control structure for the lateral controller was adopted. This led to

$$\begin{bmatrix} \delta_a \\ \delta_r \end{bmatrix} = \begin{bmatrix} K_{\text{lat}}\ K_{e_\beta}\ K_{e_p} \end{bmatrix} \begin{bmatrix} x_{\text{lat}} \\ e_\beta \\ e_p \end{bmatrix}. \tag{7}$$

As before, this controller attains ample stability margins to accommodate for filters and time delays. The anti-windup technique in [7] is applied to the $\langle e_\beta, \delta_r \rangle$ and $\langle e_p, \delta_a \rangle$ pairs.

C. Competing Control Alternatives

A single-trim-point flight controller for X^* and U^* was designed first, for a horizontal wings-level flight condition and 80 knots (41.2 m/s) air speed; the corresponding angle of attack is 4.28° and the flight path angle, γ, is zero. This controller will be denoted as $\mathcal{C}_1$. The controller gains were tuned according to classical control metrics and time responses to representative pilot commands. It is the fast modes of motion of the vehicle that are important in this process as the slower modes (in particular the spiral) can be compensated by either the pilot or an autopilot. To improve the command tracking performance outside the normal flight envelope, gain-scheduled controllers were designed [17]. One of these, denoted as $\mathcal{C}_2$ and which can be

Table 1: Bifurcation diagram notation.

———	Stable equilibrium	○	Hopf bifurcation
———	Stable 6-state equilibrium	●	Torus bifurcation
– – –	Unstable equilibrium	■	Period doubling bifurcation
———	Stable periodic orbit		
– – –	Unstable periodic orbit		

regarded as moderately aggressive in its tracking performance, is considered in this paper. This controller schedules three fixed-point controllers designed at angles of attack of $4.28°$, $13°$, and $22°$. The gains at the design point of $4.28°$ matches the gains for $\mathcal{C}_1$.

III. Bifurcation Analysis

In this section we first summarize aspects of the multi-attractor dynamics underlying the open-loop behaviour of the GTM, by means of bifurcation diagrams. We then consider how these change when the loop is closed with the controllers $\mathcal{C}_1$ and $\mathcal{C}_2$, with particular emphasis on off-nominal conditions and upset with the controller $\mathcal{C}_1$. Upset is defined in the Upset Recovery Training Aid (URTA) [18] as an inadvertent event where: (i) Pitch angle, θ, goes beyond the set $[-10°, 25°]$, (ii) Roll angle, ϕ, exceeds $\pm 45°$, (iii) or flying with an inappropriate airspeed.

The continuation parameters used in the bifurcation diagrams shown here are either the commanded angle of attack by the pilot α_{cmd} or a 'gain parameter' GP on the controller gains (defined in Section III C). The diagrams are generated with the method of numerical continuation, in this case using the software package AUTO [19] incorporated into the Matlab Dynamical Systems Toolbox [20]. The line types and symbols adopted here to define equilibria and bifurcations are listed in Table 1.

A. α_{cmd} bifurcation diagrams – controller $\mathcal{C}_1$

During the controller design, $\mathcal{C}_1$ was evaluated for a variety of $\gamma = 0°$ trims. This condition yields an implicit dependency between α_{cmd} and V_{cmd}. To replicate this, the same trim function as that adopted in the controller design was used to define a schedule of V_{cmd} inputs versus continuation parameter α_{cmd}. This

Table 2: Summary of characteristics of GTM closed-loop behaviour (controller $\mathcal{C}_1$) in Fig. 1.

Symbol	Type of dynamics	Approx. α_{cmd} range
A	Symmetric equilibria: unstable spiral	0° to 12° and 12.7° to 21°
	but fast modes (6^{th}-order system) stable	
B	Low-amplitude limit cycle in stall region	12° to 12.7°
C1	Stable equilibria: helical turn ($+\phi$)	0° to 12° and 12.7° to 20.3°
C2	Stable equilibria: helical turn ($-\phi$)	0° to 12° and 12.7° to 21°
D1	Low-amplitude limit cycle in stall region on C1	12° to 12.7°
D2	Low-amplitude limit cycle in stall region on C2	12° to 12.7°
E	Large amplitude unstable limit cycle	21° to 22.5° (aileron saturation)
F1	Large amplitude stable limit cycle from C1	20.3° to 22° (elevator saturation)
F2	Large amplitude stable limit cycle from C2	21° to 22° (elevator saturation)

schedule was then implemented during the numerical continuation runs such that V_{cmd} and, hence, throttle setting, also change as α_{cmd} varies ensuring symmetric trim solutions with $\gamma = 0^\circ$. Also, the full equation 12^{th}-order flight mechanic states described in equation (3) are reduced to eight because $[x, y, \phi]$ are decoupled from the other equations and z is only coupled through air density which changes little during flight dynamic studies. Hence, these play a negligible role in the flight dynamics behaviour of the aircraft and are neglected.

Figure 1 shows the α, p, ϕ and θ projections of the closed-loop bifurcation diagram with α_{cmd} as continuation parameter. The chosen range for α_{cmd} is 0°-30°, as this encompasses the range considered during the controller design and evaluation. The p and β projections (not shown) yield equilibrium solutions that are zero, commanded value, indicating that the p_{cmd} and β_{cmd} systems are able to meet their objective in terms of steady state behaviour throughout the α range shown. For the majority of the chosen α_{cmd} range, α also matches its target equilibria values; however, this becomes unachievable for $\alpha_{\text{cmd}} \geq 23^\circ$ on the non-symmetric branch, due to position saturation of the elevator. In this implementation, control surface position saturation is modelled by the use of smoothly blended piecewise functions. These are three linear functions blended smoothly using a hyperbolic tangent function; see Ref. [21].

The types of behaviour on the various solution branches in Fig. 1 are summarised in Table 2. The closed-

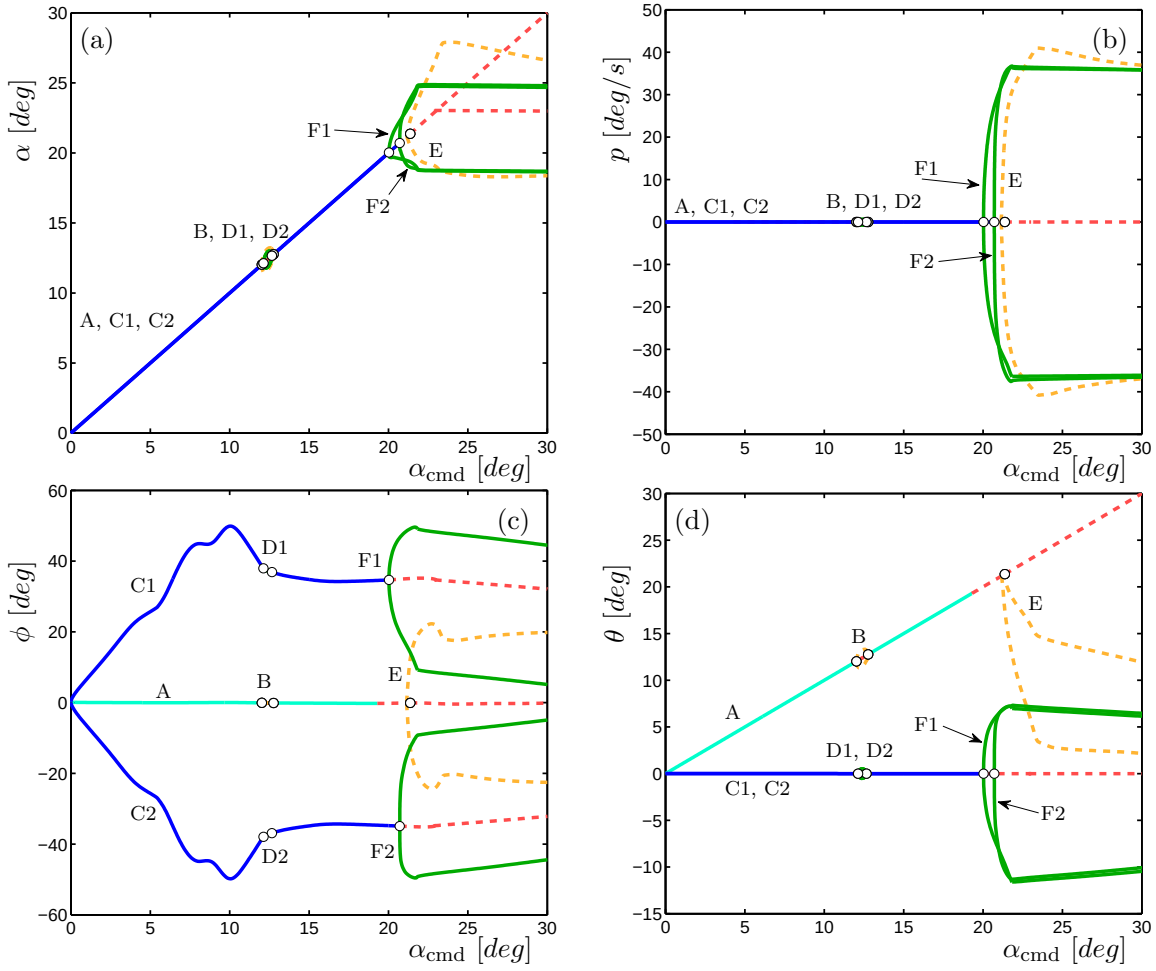

Fig. 1: Closed-loop bifurcation diagram, using $\mathcal{C}_1$, in α, p, q, ϕ, θ and δ_r, panels (a)-(f) respectively.

loop symmetric trim solution branch (marked 'A' in Fig. 1) is unstable due to the slow spiral mode. However, the time-to-double-amplitude for this mode is large: flying qualities are considered to be acceptable ('level 1' in conventional flying qualities terminology [22] which corresponds to 'satisfactory' in [23]) for α_{cmd} up to $19.3°$. Solutions meeting this time-to-double-amplitude level 1 flying qualities criterion are indicated 6-state stable using the light blue line type (shown in table 1) in the closed-loop bifurcation diagrams.

In the stall angle-of-attack region there is a further instability originating at a Hopf bifurcation at $\alpha_{\text{cmd}} = 12°$. This gives rise to periodic orbits (marked 'B') which grow in amplitude and then reduce again, disappearing in another bifurcation at $\alpha = 12.7°$. This small region of instability does represent a deficiency in the fixed-gain controller, although the consequences would not be considered dangerous in the context of loss-of-control or upset due to the low amplitude. A further Hopf bifurcation arises at $\alpha = 21°$; an unstable

limit cycle is born at this point ('E'). The aileron deflections saturate at $\alpha \approx 22.5^\circ$ and the orbits remain unstable until at least $\alpha = 30^\circ$. Analysis of the linearized system confirms that the periodic orbit B corresponds to a loss of longitudinal stability while periodic orbit E corresponds to a loss of lateral-directional stability.

In addition to the symmetric solution branch there are two branches of stable equilibria arising denoted 'C1' and 'C2'. These are close to anti-symmetric in the lateral-directional sense. Inspection of these solutions shows that they represent helical trajectories – descending turns – where $\theta = 0^\circ$. This is due to the kinematics of an aircraft constrained in a turn with zero roll rate, due to the $p_{\text{cmd}} = 0^\circ$/s function in the controller. In particular, consideration of the $\dot{\phi}$ and $\dot{\theta}$ kinematic equations at equilibrium with $p = 0^\circ$/s reveals that $r \tan\theta$ must be zero. For the symmetric solution branch A, $r = 1^\circ$/s so that $r \tan\theta$ will be zero for all θ; however, for the turning solution where $r \neq 0$, pitch angle θ must be zero for the kinematic constraint to be met. Calculation of γ confirms that these turns denote descending flight.

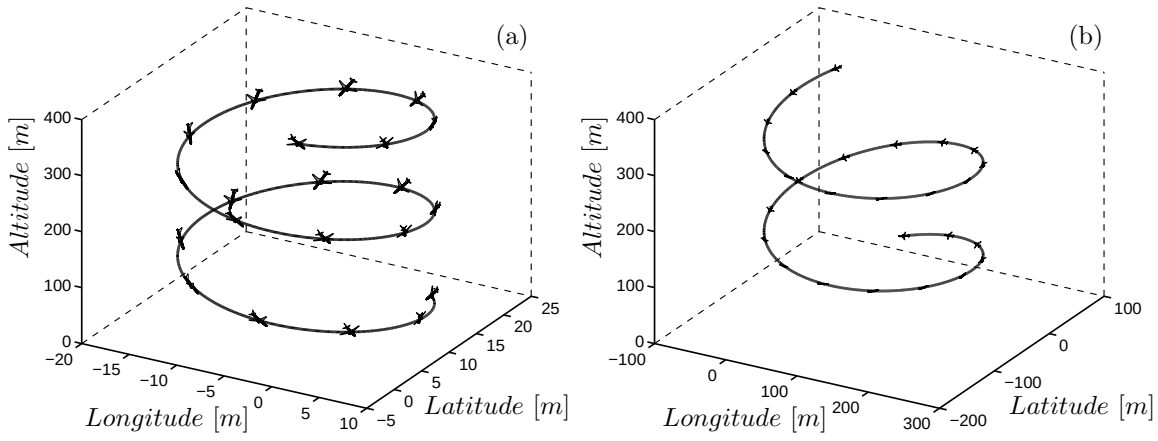

Fig. 2: Trajectories: Open-loop steep spiral (a) and closed-loop descending turn (b).

Figure 2 shows a comparison between the open-loop steep spirals with those of the closed-loop descending turns. The groundtrack radius, for the descending turns is far larger than that of the steep spiral (120.8 m compared to 11.6 m) and γ is much smaller. For helical turns, the only condition considered upset by the URTA [18] is that $\phi \geq \pm 45^\circ$. However, this is just for a small portion of the branches between $7^\circ < \alpha_{\text{cmd}} < 11^\circ$. Thus the descending turns do not reflect upset conditions for the majority of the α_{cmd} range, unlike the open-loop steep spirals, showing improved upset behaviour with the addition of controller $\mathcal{C}_1$.

As with the symmetric branch, the descending turns also lose stability in the $\alpha = 12^\circ$-12.7° range

although, again, the amplitudes of the resulting periodic orbits (D1 and D2) are small. Similarly, Hopf bifurcations points exist on these branches in the region of $\alpha_{\text{cmd}} = 20°$-$21°$. The periodic orbits (F1 and F2) that grow from them are stable; they increase in amplitude as α_{cmd} increases until the elevator and ailerons saturate during parts of the orbits (as from $\alpha_{\text{cmd}} \approx 22°$) and maintain stability until at least $\alpha_{\text{cmd}} = 30°$. Due to the large rate of change of attitude, periodic orbits F1 and F2 can be considered as potential upset solutions as this could induce excessive loads on the aircraft.

B. α_{cmd} bifurcation diagrams – controller $\mathcal{C}_2$

As described in Section II C, controller $\mathcal{C}_2$ is gain scheduled based on three trim points at angles of attack corresponding to cruise, stall and post-stall flight conditions ($4.28°$, $13°$ and $22°$, respectively). Given the bifurcation diagrams shown thus far, these design points are seen to be well suited to accommodate the nonlinear nature of the GTM dynamics and so we would expect a well-designed gain scheduled controller to stabilize the solutions through the limit cycle regions described above for the fixed-gain controller (i.e., referring to Fig. 1/Table 2, around points B, D1 and D2 in the $12°$-$13°$ angle of attack region and points E, F1 and F2 above $20°$ angle of attack).

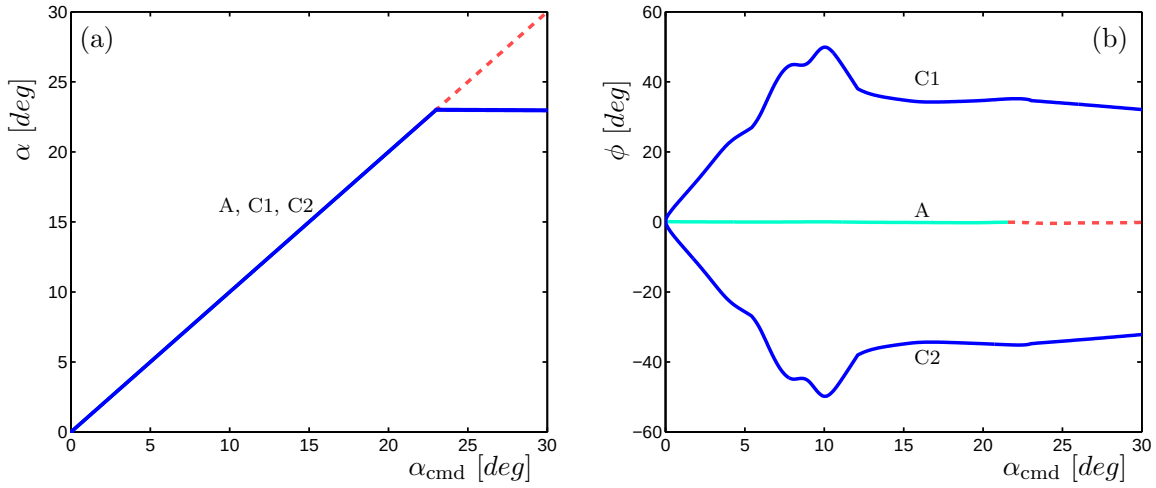

Fig. 3: Closed-loop bifurcation diagram, using $\mathcal{C}_2$, in α, p, q and ϕ, panels (a)-(d) respectively.

Figure 3 shows the α and ϕ projections of the bifurcation diagram for controller $\mathcal{C}_2$. By evaluating the time-to-double-amplitude for the unstable spiral mode, $\mathcal{C}_2$ satisfies the level 1 handling quality criterion up to a slightly higher angle of attack ($\alpha_{\text{cmd}} = 21.5°$) than $\mathcal{C}_1$. More importantly, it is evident that the gain-

scheduled controller $\mathcal{C}_2$ stabilises all the periodic orbits that were exhibited by controller $\mathcal{C}_1$. This implies that $\mathcal{C}_2$ stabilises the aircraft throughout the usable α_{cmd} range.

C. Application of the gain parameter to all controller gains

The principal interest in using bifurcation methods to assess the impact of control laws is to investigate off-nominal conditions and, in particular, the influence of attractors associated with unwanted behaviour – including upset. In order to further investigate how the open-loop system is modified by the controllers, we carry out numerical continuation with a 'gain parameter', GP, as the continuation parameter to represent the transition from open- to closed-loop. This so-called 'homotopy' parameter is simply a factor applied to one or more of the controller gains, such that when GP=0 the gains are zero (open loop) and when GP=1 the relevant gains are at their design values for the controller under consideration. This analysis enables tracking of the dynamics from open-loop to closed-loop along with exploring the stability margins of the controller as GP increases beyond 1.

Figure 4 shows this open-to-closed-loop transition when continuation parameter GP is applied to *all* the gains, i.e. those on the command paths and those on the stability augmentation paths. The continuation was initiated at GP=1 and then the gains continued in both negative and positive directions. To carry out this analysis, consideration must be given to the constant values used for the controller commands since the GP=0 and GP=1 points may be very different flight conditions. In this case, controller commands corresponding to symmetric trim at $\alpha_{\text{cmd}} = 20^\circ$ were chosen, because this was close to the point of lateral-directional instability that manifests itself in periodic orbits E, F1 and F2 in Fig. 1. As the gain parameter is varied, the controller commands remained fixed at their $\gamma = 0$ trim settings for $\alpha = 20^\circ$. This gives rise to an 'instantaneous' demand on the controlled variables as soon as GP increases above zero. The periodic solutions which would arise from the Hopf bifurcations have not been considered here, as the primary interest for the design of controller gains is the point where stability is lost rather than the behaviour past this point. However, this stability would be recoverable a reduction of α_{cmd}.

It is evident from Fig. 4 that, when the controller is operative (GP>0), it attempts to drive the states to the pilot commands, even when the gain is very small. This results in a very dramatic change in the equilibrium solutions as the gain increases slightly from zero. The state variables move to the commanded values while

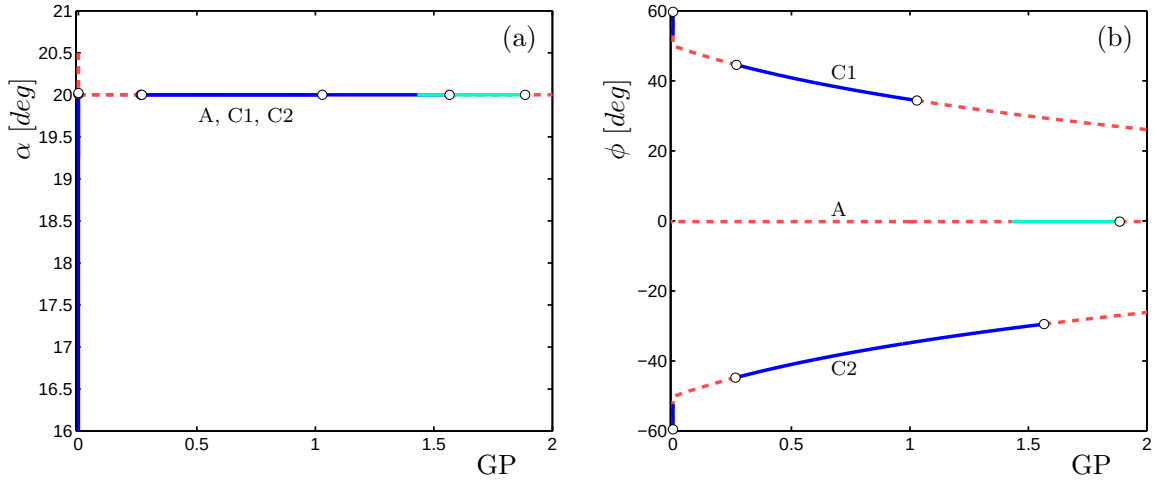

Fig. 4: Closed-loop bifurcation diagram, using $\mathcal{C}_1$,with continuation in gain parameter GP.

the other uncommanded states vary as GP varies and reach the full closed-loop values when GP=1. At small gains (where GP≤ 0.25), stability is lost on all three branches at Hopf bifurcations. For larger gains, if GP is increased just beyond a value of 1, the C1 (positive ϕ) turning solution loses stability at a Hopf bifurcation indicating that, at this point, controller $\mathcal{C}_1$ has limited stability margin. The branch C2 (negative ϕ) does not lose stability until GP ≥ 1.55, which shows that the descending turn with negative ϕ is a more robust solution than that for positive ϕ. This difference is likely due to the asymmetry of the GTM rather than the controller. The loss of stability of C1 so close to the nominal controller gains would not be expected – although it is clear that the controller $\mathcal{C}_1$ is operating far away from the design point of $\alpha = 4.28°$. Figure 4 also indicates that to achieve level 1 spiral mode flying qualities on the symmetric branch for $\mathcal{C}_1$ at $\alpha = 20°$, the parameter GP needs to be in excess of about 1.45 (cf. Fig. 1 where the spiral mode rate of divergence no longer meets level 1 handling quality levels once α_{cmd} exceeds $19.3°$).

The gain parameter bifurcation diagram for the controller $\mathcal{C}_2$, Fig. 5, exhibits similar behaviour to that for $\mathcal{C}_1$. Due to the gain-scheduling design point at $\alpha = 22°$, the gains of this controller are more optimal at $\alpha_{\text{cmd}} = 20°$ than those of $\mathcal{C}_1$ and, hence, the system loses stability on the descending turn branches only once GP is reduced below about 0.15 while maintaining stability until at least GP=2. Also, for the symmetric branch, controller $\mathcal{C}_2$ maintains level 1 flying qualities for GP values down to approximately 0.5 showing superior robustness at high α to $\mathcal{C}_1$.

In terms of flight upset, of greater concern is the impact of both the controllers on the oscillatory spin

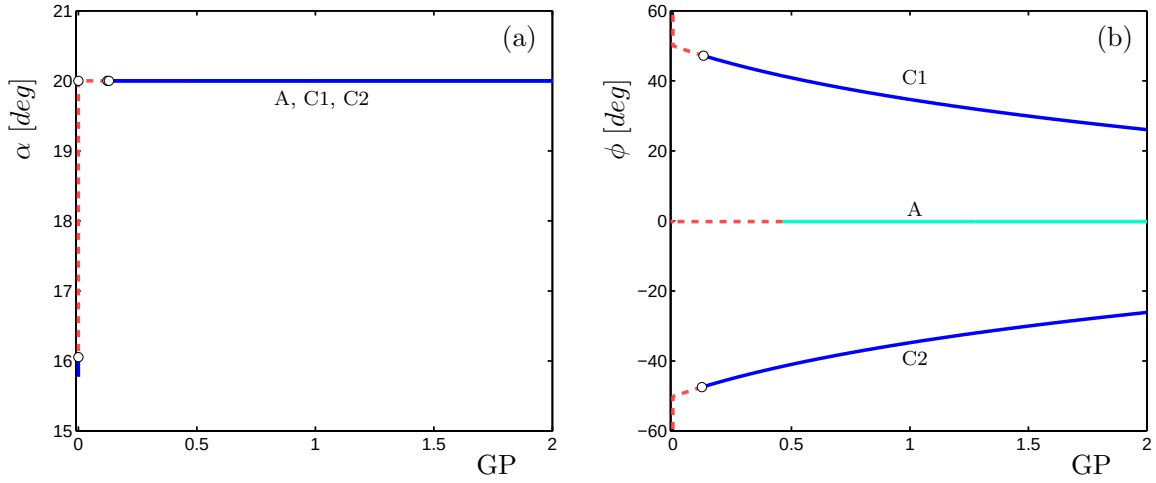

Fig. 5: Closed-loop bifurcation diagram, using $\mathcal{C}_2$,with continuation in gain parameter GP.

solutions (regimes F and G in Fig. 1) that are present in the open-loop system. The bifurcation diagrams of the closed-loop system for both $\mathcal{C}_1$ and $\mathcal{C}_2$ imply that the GTM does possess sufficient control authority to allow the command path to eliminate the oscillatory spins as these solutions could not be located. We now look at pairing back the controller to investigate how these open-loop dynamic regimes are eliminated.

D. Application of the gain parameter to stability augmentation gains

In order to further investigate the impact of the control law on the spin regime and to assess the attributes of the bifurcation method, the gain parameter method described earlier was applied to the stability augmentation path of the controller only. The command path integrator gains and the auto-throttle were disabled. The stability augmentation path uses purely proportional gains and consists of a total of nine separate paths. Both longitudinal and lateral-directional stability augmentation gains were used. We refer to this combination of gains as the 'proportional gains' and the gain parameter applied to them as GP_{SA}.

Figure 6 shows the α, p, ϕ and δ_r projections of a bifurcation diagram for controller $\mathcal{C}_1$ in which GP_{SA}, applied to all proportional gains, is varied from 0 up to 1 (recalling that GP_{SA}=1 corresponds to the $\mathcal{C}_1$ design gain values). When GP_{SA}=0, the solution branches are equivalent to that of the open-loop system bifurcation diagram at $\delta_e = -24°$. The value of $\delta_e = -24°$ was chosen because, at this elevator deflection, both the open-loop steep spins, regimes F and G, are stable as are the steep spirals. The solution branch labels in Fig. 6 correspond to those for the open-loop system described in table 3 due to the deactivation of the command

Table 3: Characteristics of GTM open-loop behaviour.

Symbol	Type of Dynamics	α range
C	Steady steep spiral	10.5° to 20.9°
D	Inverted spiral	-5° to -2°
E	Steady steep spin	30.5° to 38.8°
F	Period-one oscillatory steep spin	32.7° to 38.5°
G	Period-three oscillatory steep spin	30.8° to 40°

path. It is evident that closing the loop for a set of suitable controller gains ($\text{GP}_{\text{SA}} \geq 0.35$) does eliminate the spin branches: they all undergo limit point bifurcations as GP is increased. Further analysis, using each individual gain as the continuation parameter, has revealed that the dominant gain in the elimination of the oscillatory spins is that of proportional yaw rate feedback to the rudder. Similar behaviour is also exhibited by $\mathcal{C}_2$ [21].

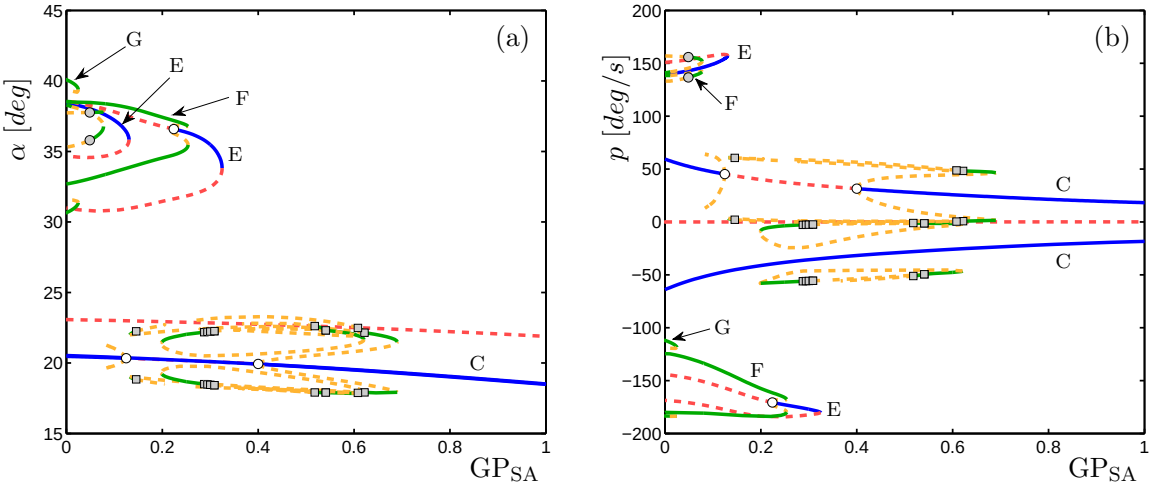

Fig. 6: Closed-loop bifurcation diagram, using $\mathcal{C}_1$ with $\alpha_{\text{cmd}} = -24^\circ$, continuation in GP_{SA}.

The negative roll rate spiral equilibrium solution branch remains stable throughout, whilst the positive roll rate equivalent includes an unstable region bounded by Hopf bifurcations. Continuing from the Hopf bifurcation (at GP_{SA}=0.4) reveals that the resulting periodic orbit grows in amplitude very significantly. It is unstable until a limit point bifurcation is reached at GP_{SA}=0.68; the stable limit cycle that arises at the fold

then exhibits multiple period doubling bifurcations as GP_{SA} decreases, indicating the presence of complex dynamics.

The above analysis shows that the proportional gain path alone is capable of eliminating both the steady spins and oscillatory spins which represent the most severe forms of upset that the GTM experiences in open-loop form. However, if they are not of a large enough magnitude, then large amplitude periodic orbits can exist on the spiral branches.

IV. Concluding Remarks

Bifurcation analysis has been used to evaluate how the flight control system alters the steady-state dynamics of the Generic Transport Model (GTM) throughout its flight envelope. Fixed-gain and gain-scheduled versions of a linear quadratic regulator controller with proportional and integral components, designed to improve the behaviour of the GTM, were studied. We focused on assessing the influence of the control laws not only for conventional symmetric trimmed flight but on off-nominal conditions too. In the results presented here, the steep spiral exhibited by the open-loop GTM is transformed into a descending turn and the oscillatory spins are eliminated. An oscillatory turn, however, is induced for the fixed-gain controller, $\mathcal{C}_1$, and exists in the form of an unacceptable oscillatory response when the loop is closed. This behaviour is not observed for the gain-scheduled controller, $\mathcal{C}_2$.

By conducting bifurcation analysis with respect to a homotopy parameter acting on one or more of the controller gains, we were able to gain insight into the effect of changes to the controller on the closed-loop dynamics. This was illustrated in terms of the proximity to the closed loop limit cycles above 21° angle of attack for the fixed- gain controller, and the changes in co-existing steep spiral and oscillatory spin branches caused by tuning proportional gains. Our analysis also shed light on the robustness of the controllers and information on how the controllers modify the open-loop upset dynamics. Since most controllers are not designed to cope with upsets, the reported analysis approach can be used to evaluate their effectiveness under operating conditions encountered during off-nominal, strongly nonlinear flying conditions. This could potentially be used to determine certain situations when it is beneficial to turn the controller off to recover from an upset.

Acknowledgements

The research of Stephen J. Gill was supported by a UK Engineering and Physical Sciences Research Council (EPSRC) studentship in collaboration with Airbus. We are grateful to colleagues in the NASA Langley Flight Dynamics Branch and Dynamics Systems and Control Branch for provision of the Generic Transport Model and advice on its use. This work collaboration was supported by the Royal Society International Exchanges Scheme grant no. IE121367.

References

[1] Chatrenet, D., "Air Transport Safety - Technology and Training," *ETP 2010*, 2010, URL: http://ec.europa.eu/invest-in-research/pdf/workshop/chatrenet%20_b3.pdf [cited 10 June 2014].

[2] Aviation Safety Boeing Commercial Airplanes, "Statistical Summary of Commercial Jet Airplane Accidents Worldwide Operations 1959 - 2012," Tech. rep., Boeing Commercial Airplanes, 2013.

[3] Balas, G. J., "Linear, Parameter-Varying Control and its Application to Aerospace Systems," *23rd Congress of International Council of the Aeronautical Sciences*, 2002, ICAS 2002-5.4.1.

[4] Khalil, H. K., *Nonlinear Systems: Pearson New International Edition 3rd Edition*, No. ISBN 978-1292039213, Pearson, Edinburgh Gate, Harlow, Essex, CM20 2JE, UK, 2002.

[5] Friedman, A., "Dynamic Inversion and Control of Nonlinear Systems," *Mathematics in Industrial Problems*, edited by A. Friedman, No. ISBN 978-1-4615-7401-9 in The IMA Volumes in Mathematics and Its Applications, Springer-Verlag New York, Inc., 175 Fifth Avenue, New York, NY 10010, USA, 1988, pp. 114–120, DOI 10.1007/978-1-4615-7399-9.

[6] Gregory, I. M., Cao, C., Xargay, E., Hovakimyan, N., and Zou, X., "L1 Adaptive Control Design for NASA AirSTAR Flight Test Vehicle," *AIAA Guidance, Navigation, and Control Conference*, 2009, AIAA-2009-5738, DOI 10.2514/6.2009-5738.

[7] Crespo, L. G., Matsutani, M., and Annaswamy, A., "Design of an Adaptive Controller for a Remotely Operated Air Vehicle," *Journal of Guidance, Control, and Dynamics*, Vol. 35, No. 2, 2012, pp. 406–422, DOI 10.2514/1.54779.

[8] Jordan, T. L., Foster, J. V., Bailey, R. M., and Belcastro, C. M., "AirSTAR: A UAV Platform for Flight Dynamics and Control System Testing," *AIAA Aerodynamic Measurement Technology and Ground Testing Conference, San Francisco, CA*, June 2006, AIAA-2006-3307, DOI 10.2514/6.2006-3307.

[9] Foster, J., Cunningham, K., Fremaux, C., Shah, G., Stewart, E., Rivers, R., Wilborn, J., and Gato, W., "Dynamics Modeling and Simulation of Large Transport Airplanes in Upset Conditions," *AIAA Guidance, Navigation, and Control Conference*, San Francisco, CA, August 2005, AIAA-2005-5933, DOI 10.2514/6.2005-5933.

[10] Abramov, N., Goman, M., Khrabrov, A., Kolesnikov, E., Fucke, L., Soemarwoto, B., and Smaili, H., "Pushing Ahead – SUPRA Airplane Model for Upset Recovery," *AIAA Modeling and Simulation Technologies Conference*, Minneapolis, MN, August 2012, AIAA-2012-4631, DOI 10.2514/6.2012-4631.

[11] Goman, M., Zagainov, G., and Khramtsovsky, A., "Application of Bifurcation Methods to Nonlinear Flight Dynamics Problems," *Prog. Aerospace Sci.*, Vol. 33, 1997, pp. 539–586, DOI 10.1016/S0376-0421(97)00001-8.

[12] Thompson, J. and Macmillen, F., editors, *Nonlinear flight dynamics of high-performance aircraft*, The Royal Society, Theme Issue, Phil. Trans. R. Soc. Lond. A, Vol. 356, No. 1745, Oct., 1998.

[13] Gill, S. J., Lowenberg, M. H., Neild, S. A., Krauskopf, B., Puyou, G., and Coetzee, E., "Upset Dynamics of an Airliner Model: A Nonlinear Bifurcation Analysis," *Journal of Aircraft*, Vol. 50, No. 6, 2013, pp. 1832–1842, DOI 10.2514/1.C032221.

[14] Crespo, L. G., Kenny, S. P., Cox, D. E., and Murri, D. G., "Analysis of Control Strategies for Aircraft Flight Upset Recovery," *AIAA Guidance, Navigation, and Control Conference*, 2012, AIAA-2012-5026, DOI 10.2514/6.2012-5026.

[15] Cunningham, K., Cox, D. E., Murri, D. G., and Riddick, S. E., "A Piloted Evaluation of Damage Accommodating Flight Control Using a Remotely Piloted Vehicle," *AIAA Guidance Navigation and Control Conference, Portland, OR*, August 2011, AIAA-2011-6451, DOI 10.2514/6.2011-6451.

[16] Murch, A. M., "A Flight Control System Architecture for the NASA AirSTAR Flight Test Infrastructure," *AIAA Guidance Navigation and Control Conference, Honolulu, HI*, August 2008, AIAA-2008-6990, DOI 10.2514/6.2008-6990.

[17] Rugh, W. J. and Shamma, J. S., "Research on Gain Scheduling," *Automatica*, Vol. 36, No. 10, 2000, pp. 1401–1425, DOI 10.1016/S0005-1098(00)00058-3.

[18] Carbaugh, D. and Rockliff, L., "The Airplane Upset Recovery Training Aid, Revision 2," 2008, URL: http://flightsafety.org/archives-and-resources/airplane-upset-recovery-training-aid [cited 17 July 2014].

[19] Doedel, E. J. and Oldeman Bart, E., "AUTO-07P: Continuation and Bifurcation Software for Ordinary Differential Equations," Tech. rep., http://sourceforge.net/projects/auto-07p/files/auto07p/ [retrieved 11 August 2014], Jan. 2012.

[20] Coetzee, E., Krauskopf, B., and Lowenberg, M., "The Dynamical Systems Toolbox: Integrating AUTO into Matlab," *16th US National Congress of Theoretical and Applied Mechanics*, No. USNCTAM2010-827, USNCTAM, Pennsylvania State University, PA, June-July 2010.

[21] Gill, S. J., *Investigation into upset and upset recovery using bifurcation analysis*, PhD dissertation, Bristol University, Department of Aerospace Engineering, 2014.

[22] Cook, M. V., *Flight Dynamics Principles*, No. ISBN 0 340 63200 3, Arnold, 338 Euston Road, London, NW1 3BH,

UK, 1997.

[23] Cooper, G. E. and Harper Jr., R. P., "The use of Pilot Ratings in the Evaluation of Aircraft Handling Qualities," Technical Note TN D-5153, NASA, 1969.